Albuquerque Academy Team 1

Additive Manufacture Kinetics and Thermodynamics Model

New Mexico

Supercomputing Challenge

Final Report

April 25, 2025

AA Team 1

Albuquerque Academy

Created by

Harrison Schiek

Teacher Mentors

Jay Garcia

Alex Benedict

Table of Contents ------------------------

Executive Summary ----------------------

Problem

As Additive Manufacturing (AM) and, more specifically, Fused Filament Fabrication (FFF) grow in importance and prevalence, it is essential to understand bonding conditions for materials and resultant material strength. Especially for high-strength applications like aerospace and construction and high-precision applications in nanotech and biomaterials, manipulation and careful characterization of materials is crucial. With its introduction into these fields, AM will lower costs and break down barriers for research and innovation. It is essential to expand support for AM applications through bettering understanding for improved material effectiveness.

Solution and Methodology

The filament was modeled as a set of non-colloidal particles using Molecular Dynamics and other interactions. Two kinds of exchange occur between nodes of the simulation; the first being thermal energy, and the second being kinetic energy. To model the first, the Heat Equation was applied using simple approximations of the second derivative. For kinetic exchanges, Lennard Jones potentials, friction, and torque captured the interaction with high fidelity. Temperature was also included in gauging friction and bond potential energy to increase accuracy. To evaluate bonding strength, measured temperature and strain during solidification contributed to an aggregate measure for characterization thereof.

Validation and Verification

By testing each component of the model in individualized trials, the model is shown to accurately predict logical results and textbook examples. To further verify their effectiveness, material characterizations were compared with literature material properties at temperature.

Results

The model indicates two major changes to improve FFF material effectiveness. The first change is higher plate temperature. This provides for the slow and steady bonding of the material. The second conclusion is that effective high temperature control of the bonding surface increases bonding quality, as maintaining even high temperature ensures key interlayer bonding.

Problem ------------------------------------

There are myriad reasons to value AM highly as a target for not only research but also investment. AM isn't a new idea, but many of its extensions and specializations, especially FFF, have grown immensely in recent years and show promise to revolutionize numerous industries that were previously unaffected by this type of manufacture. Lack of understanding now prevents broader applications, as gaps in precision and material strength limit usability. Overall, due to AM's growth, versatility, and environmental importance, it is essential to better understand and characterize bonding and product strength to broaden its impact.

AM technology has grown at an unprecedented rate and is projected to continue this growth. Specifically, growth of the global industry for AM from 2023 to 2030 is estimated to be 432.75% (around 23.3% annually)[1]. Importantly, FFF is the second largest contributory sector of AM[1].This growth makes it essential to support AM and FFF with better understanding and tools to predict performance. By facilitating more effective use of AM, greater uptake and positive effects will be seen across numerous industries. AM is also expanding into numerous new fields, where it promises to remove impediments to research and production. An article summarizing AM and its current uses states, "[AM] is rapidly expanding to a large number of industrial sectors such as aeronautics, automobile and biomedicine, with significant growth in the medical device and wearables markets"[2]. Given the wide spanning reach with an emphasis on precision and strength, predicting and printing for specific characteristics is crucial. Additionally, by improving understanding, problems with bonding and product durability will be reduced in severity. To empower the transition to AM, it is invaluable to improve understanding to reduce waste and cost and develop overall quality.

AM's versatility makes it crucial for large scale implementation. FFF machinery and equipment are almost independent of design, meaning costly specialization by product is nearly nonexistent. This allows flexibility for producers, lowering costs for experimentation and development. In addition, this makes much more possible for scientists. NASA highlights the importance of AM coupled with Thermodynamic modeling software specifically: "Applying these two processes (Thermodynamic Modeling and 3D Printing) has drastically accelerated the rate of our materials development. We can now produce new materials faster and with better performance than before"[3]. As seen here, effective modelling crucially streamlines development

processes and better supports science and industry. Adding on, a report by the US Department of Commerce notes the utility of AM in a broad variety of new uses due to its versatility. It states, "[AM] can facilitate the customized production of strong light-weight products"[4]. The wide spanning uses of AM as a result of its versatility illuminate the importance of utilization with confidence.

AM results in far less production waste, energy cost, and raw material usage. Its implementation will lead the way to importantly reducing the significant industrial burden on the environment. A paper, published in the journal *Advanced Industrial and Engineering Polymer Research*, focusing on AM as a sustainable manufacturing alternative reveals that AM results in "lesser material waste, energy usage, and machine emissions" as opposed to current manufacturing techniques[5]. Given these profound benefits over currently prevalent methods, the use of AM technologies to reduce overall pollution is promising. In the ongoing fight against Climate Change, the effective implementation and development of AM is a crucial step. The same paper emphasizes AM's importance in long term sustainability and climate efforts[5]. AM technologies play an important role as a more sustainable and environmentally friendly means of manufacture, and it is essential to support broad application and implementation.

Methodology and Algorithms -----------

The model consists of two major methods of energy exchange between nodes: thermal energy exchange and a kinetic energy exchange. Each of these methods will be examined in depth through foundations in established theory to implementation and program calculation. First, though, a description of the model framework and setting will set the stage for algorithmic usage and its computational effectiveness.

The model was developed from scratch exclusively in python using text editor BBEdit. It was run predominantly on a desktop computer with 3.4 GHz 8 Core Processor and a portable computer with 4.05GHz 8 Core Processor. Significant Python libraries Matplotlib and NumPy were used, the first for visualizations and the second for arrays and data organization. The model uses a Modelling by Decomposition approach to model a complicated 3D printed solid. It uses a hexagonal matrix of points to approximate the whole solid, and it manages internodal interactions by defining adjacency by spacing and considering only directly adjacent interactions.

The nodes can be thought of as small pieces of the whole not in any particular shape. As an example of adjacent nodes see Figure 1. The red node gives an example node and the orange nodes give all the adjacent nodes. The definition is just within 1.5 units of distance.
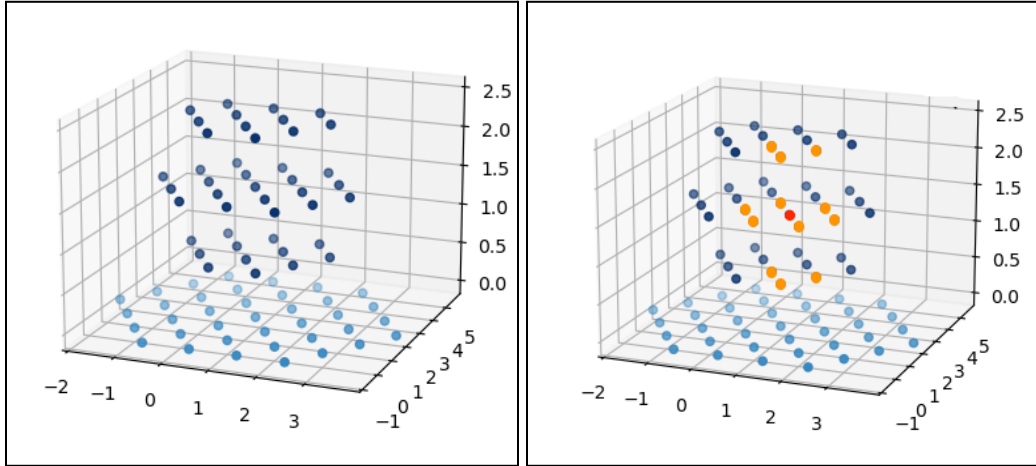
(Fig. 1)

Heat Exchange

The first physics feature of interest is heat exchange. To model this interaction, the Heat Equation was modified and applied to this nodal approach. Since the framework considers specifically particle-on-particle interactions, the complexity of the 3D Heat Equation was somewhat generalized for usage. A single variable r can represent distance between particles and replace position variables x, y, and z. t gives time. T gives the temperature, which is a function of x, y, z, and t. α is the thermal diffusivity. See Equation 1-1:

$$\frac{\delta T}{\delta t} = \alpha \nabla^2 T = \alpha\left(\frac{\delta^2 T}{\delta x^2} + \frac{\delta^2 T}{\delta y^2} + \frac{\delta^2 T}{\delta z^2}\right) = \alpha\frac{\delta^2 T}{\delta r^2} \qquad (1\text{-}1)$$

To adapt the equation further for use in the simulation, gaining an approximation of the second derivative for a point is crucial. To do this, consider (in only one dimension for simplicity) three nodes of temperatures T_1, T_2, and T_3, and positions x_1, x_2, and x_3. Approximating the first

derivative on the two sections, the two approximations are given by equations 1-2. The approximation is simply the equivalent of change in T over change in x for the function.

$$\frac{\delta T}{\delta x}\bigg|_1 \approx \frac{T_2 - T_1}{x_2 - x_1} \qquad\qquad \frac{\delta T}{\delta x}\bigg|_2 \approx \frac{T_3 - T_2}{x_3 - x_2} \tag{1-2}$$

Again using the same idea to approximate the second derivative at the center of the full interval and making the simple assumption that these particles are at the same distance from the central node (calling this distance r), the simplification and separation of interactions is shown (Eq. 1-3).

$$\frac{\delta^2 T}{\delta x^2} \approx \frac{\dfrac{T_3-T_2}{x_3-x_2} - \dfrac{T_2-T_1}{x_2-x_1}}{\dfrac{x_3+x_2}{2} - \dfrac{(x_2+x_1)}{2}} = \frac{\dfrac{T_3-T_2}{r} - \dfrac{T_2-T_1}{r}}{\dfrac{2r+x_2+x_1}{2} - \dfrac{(x_2+x_1)}{2}} = \frac{T_3-T_2}{r^2} + \frac{T_1-T_2}{r^2} \tag{1-3}$$

This shows the final simplification and manipulation of the heat equation for use in one-on-one particle interactions. Equation 1-3 really shows how the change in temperature at a point is given in approximate by the sum of nodes around in their change in temperature divided by the square of the distance, thus making these interactions simply calculable for any given set of nodes. See Equation 1-4 for the final usage of the Heat Equation, with Particle 1 being the particle from who's reference the calculations are made and Particle 2 being a particle adjacent to Particle 1 and thus included in the calculations. (Subscripts giving attributes of the particles and r being distance between particles). This is applied to a collection of nodes in 3D in the program.

$$\frac{\delta T}{\delta t}\bigg|_{part} = \alpha\frac{\delta^2 T}{\delta r^2} \approx \alpha\frac{T_2 - T_1}{r^2} \qquad\qquad \frac{\delta T}{\delta t}\bigg|_{tot} = \sum_{n=2} \alpha\frac{T_n - T_1}{r_n^2} \tag{1-4}$$

Using this relation, the model calculates heat flow from the difference in temperature and the distance between particles accurately.

Simple Internodal Forces

Next, the Lennard Jones Potential and its application will be discussed. The 12-6 Lennard Jones Potential has long been a precise way to model the intermolecular forces of very small particles. It gives the potential energy as a function of distance with several constants to control the depth of the potential energy well (the strength of the interparticle attraction or bond) and the distance of lowest potential. In this way, the equation can be adapted generally, and overall, inclusion was simple. See Equation 2-1 for constant choice.

$$V_{LJ} = 4\varepsilon\left(\left(\frac{\sigma}{r}\right)^{12} - \left(\frac{\sigma}{r}\right)^6\right) = 4\varepsilon\left(\frac{1}{4r^{12}} - \frac{1}{2r^6}\right) \qquad (2\text{-}1)$$

Important to note: Despite the V, the Lennard Jones is not an electric potential.

This is the substitution of σ for $2^{\frac{-1}{6}}$ and leaving ε (depth of the potential well) variable for implementation as a function of temperature. The idea being that, with lower temperature, there is less (unshown) thermal kinetic energy fighting the attractive force, and thus, the overall observed bond potential energy will increase. A simple approximation of this phenomenon was used, given the glass transition temperature (T_g) (Eq. 2-2). E gives the preset bond energy, which, for the coarse grain of the model, can be approximated from state changes for the material in questions and also experimental results. Specific data and implementation are discussed later.

$$\varepsilon = E\left(\frac{4T}{T_g} - 3\right)^{-1} \qquad (2\text{-}2)$$

An important characteristic of this approximation is that it gives simply E for $T=T_g$. I.E. setting E will depend on what properties the material exhibits as it approaches its brittle 'glass' state before any temperature related changes occur to its chemical structure. Another important differentiation is that for the model, this approximation of bond energy is only used when $T>T_g$. Once $T<T_g$, the model diverts calculations to a different method as will be discussed. This function maps to this concept for thermal structural changes of polymeric materials (Figure 2).
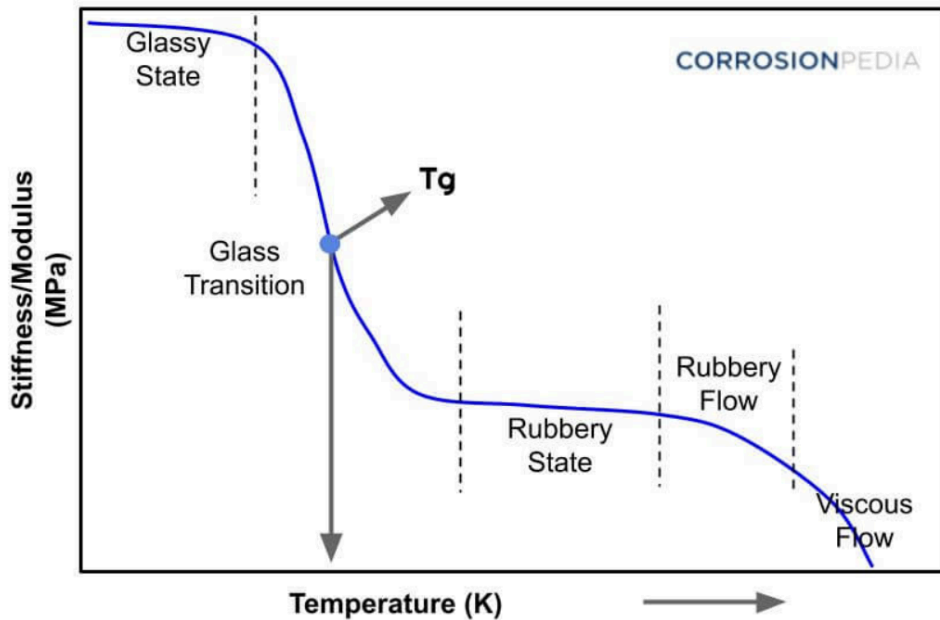
(Fig. 2)[6]

When passing the Glass Transition Temperature from hot to cold, the material loses its malleability and becomes stiff. To model this change in properties, when particles in the simulation cross this temperature they solidify their bonds and become resistant to change. The most important means of doing this is in the reevaluation of force relations with adjacent nodes. Whatever the distance between the particles is, a new Lennard Jones potential is made with the new distance as the location of the potential well, and the new potential well depth as the current potential of the node based on the old Lennard Jones. See Figure 3 where the original potential is shown in red and the new potential (of a particle bound too far at a distance of 1.3) is shown in blue. Note the new depth of the potential and the location of its well. This process is a bit abstract, but in total, it is setting forces to zero for a new configuration and weighting the strength of these 'new' bonds on how strained they were before solidification. The factoring of current strain into future bond strength is crucial. This measure of strain is also used later for evaluation of bond quality.
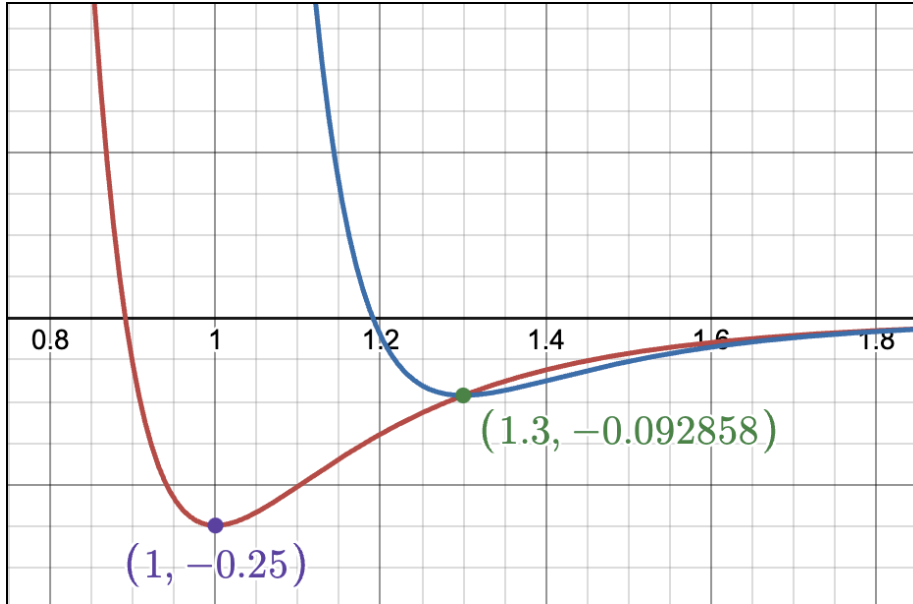
(Fig. 3)

This well approximates several characteristics of polymers, specifically storing stress while 'solidified' and becoming resistant to any change once cooled. The math to create this in the model is fairly simple. The potential and distance at the time of 'solidification' are recorded. And used in this form to yield the new Lennard Jones Potential on demand. See Equation 2-3. Where old distance is given as *d*, the old potential is given as $V_{old}(distance)$, and r is the current distance.

$$V_{new} = 4\varepsilon\left(\frac{1}{4(r+1-d)^{12}} - \frac{1}{2(r+1-d)^6}\right)\frac{V_{old}(d)}{v(1)}$$

$$V_{new} = 4E\left(\frac{1}{4(r+1-d)^{12}} - \frac{1}{2(r+1-d)^6}\right)\frac{V_{old}(d)}{4E}$$

$$V_{new} = V_{old}(d)\left(\frac{1}{4(r+1-d)^{12}} - \frac{1}{2(r+1-d)^6}\right) \qquad (2\text{-}3)$$

This process is simply moving the well and changing its depth as seen here. Additionally, there is a small shift in the d to account for thermal warping. Of course, this is just a potential and does not immediately apply to the model. A derivative is necessary to make a relevant force for computation. See Equations 2-4 for the final implementations.

9

$$F_{old} = \frac{dV}{dr} = 12\varepsilon\left(\frac{1}{r^7} - \frac{1}{r^{13}}\right) \qquad (2\text{-}4)$$

This equation gives an accurate force between nodes of the simulation and allows for kinetic exchange. However, this isn't the whole picture.

Complex Internodal Forces

Friction (or really drag) plays an important role in more concretely understanding these interactions at a coarser incrementation of distance. To gain a finer understanding without modelling millions of nodes, these additional calculations account for more properties. The model operates under a simple assumption that drag of a node operates like a Newtonian flow over its surface. Equation 3-1 gives the relevant drag equation (for flow over a surface giving net force on the ground) more clearly with $\widehat{\Delta v}$ giving the vector difference in velocities**, $\hat{d}$ giving the distance vector, $\widehat{F_f}$ giving the force vector from friction, η being the viscosity, and A being the contact area. The viscosity is changed with temperature using the same algorithm as the bond energy.

$$\widehat{F_f} = -\frac{\eta\widehat{\Delta v}}{|\hat{d}|} \cdot A \qquad (3\text{-}1)$$

One question about this assumption is should the difference velocity be considered regardless of the direction of the considered particle. An alternative projects the velocity to the distance and takes the orthogonal component to consider (Eq. 3-2).

$$\widehat{F_f} = -\frac{\eta A}{|\hat{d}|}\left(orth_{\hat{d}}\widehat{\Delta v}\right) = -\frac{\eta A}{|\hat{d}|}\left(\widehat{\Delta v} - \frac{\hat{d}\cdot\widehat{\Delta v}}{|\hat{d}|^2}\hat{d}\right) \qquad (3\text{-}2)$$

This supplies a different approach, which separates motion directly toward or away the particle

** Unfortunately, this software doesn't support conventional vector notation, so this will show vectors.

in question from motion in the perpendicular plane. This makes more sense for smaller and smaller objects, but for this coarse grid, it makes more sense to include all directions given that the contact of these particles will not only resist perpendicular motion but also motion in the direction of the other node. Combined with the increased computational weight, this specification was not included. While this force was directly applied to the nodes, it is important to note that this force is applied off-center of the node, so angular momentum is relevant and needed. Using standard formulas for Torque, calculations for angular acceleration can be used. See Equation 3-3 with $\hat{\tau}$ as the torque vector. The distance is divided by two since the interaction occurs in the middle of the two particles.

$$\hat{\tau} = \frac{\hat{d}}{2} \times \widehat{F_f} \tag{3-3}$$

This is converted pretty simply to angular acceleration by using the moment of inertia for a sphere of evenly distributed mass. See Equation 3-4. I is the moment of inertia. M is the mass of the node. $\hat{\alpha}$ is the acceleration vector.

$$\hat{\alpha} = \frac{\hat{\tau}}{I} = \frac{\frac{\hat{d}}{2} \times \widehat{F_f}}{\frac{2}{5} M \left| \frac{\hat{d}}{2} \right|^2} \tag{3-4}$$

Now that the angular velocity of the nodes has been established, a look back at the calculation of the net velocity of a nodal interaction for the definition of friction. Since each node is rotating, the observed velocity is different at each radial direction. Thankfully, this is calculated very cleanly using vector algebra. See Equation 3-5 for the definition of surface velocity from angular velocity. ω gives angular velocity (the resultant quantity of the angular acceleration shown in 3-4).

$$\widehat{v_s} = \hat{\omega} \times \frac{\hat{d}}{2} \tag{3-5}$$

This makes a net velocity calculation rather simple (Eq. 3-6)

$$\Delta \hat{v} = \hat{v}_{sA} - \hat{v}_{sh} + \hat{v}_A - \hat{v}_h \qquad (3\text{-}6)$$

This wraps up all sophisticated nodal interaction. These methods approximate the real interactions of parts within the system and lead to an accurate prediction.

Evaluation

When a node crosses the aforementioned glass transition temperature, the model grades the quality of the bonds, but to gauge what results in the actual and necessary effective bonding, it is important to define what leads to effective bonding in the first place. For this model, two major contributing factors were identified.

The first is the evenness of cooling. In modern manufacturing, the first issue is preventing uneven cooling. As summarized by industry manufacturer ZhongDe: "[It is essential] to solidify uniformly and minimize internal stresses, preventing issues like warping, shrinkage, and part deformation"[7]. Identifying uneven temperature during bonding is crucial as it leads specifically to material weakness and point failure. Specifically, a study of plastic composite cooling and solidifying highlights, "high cooling rates … cause uneven material shrinkage across different parts and pronounced warping defects"[8]. The model accounts for this process on a large scale by including thermal deformation on bonding, but finer details of temperature-related bonding are also captured. The model on grading inspects adjacent nodes and compares temperatures to the bonding temperature. The scale (S_T) gives high values for adjacent temperatures (T_a) near the bonding temperature (T_g) and lower scores for changes up or down (Eq. 4-1).

$$S_T = 10 - \left| T_g - T_a \right| \qquad (4\text{-}1)$$

This positively reports temperatures close to the glass transition temperature and successfully identifies bonding situations where the particles are not at ideal temperatures such that warping and diminished strength are problems.

The second factor is residual stress during solidification. Many materials and especially plastics 'store' their stress in their material lattice structure when solidified under stressing conditions. These stresses impact their material properties lastingly. In the ScienceDirect chapter on Tensile Residual Stress, its effects are summarized: "Tensile residual stress often induces environmentally assisted cracking and fatigue crack initiation, resulting in crucial damage"[9]. To include the factoring of stress into the model and its grading of bonding a comparison of bond potential gives the necessary detail. The algorithm calculates the bond potential and compares it to the maximum potential to obtain a measure of its closeness in energy to the optimal bonding scenario (Eq. 4-2). S_S gives the stress score; V_{old} gives the original Lennard Jones Potential, and d gives the distance at which the nodes solidified (crossed the glass transition temperature). In essence this measures the potential of the bond and compares it to the maximum potential it could have, giving 1 for a perfect length bond and numbers less than one for strained bonds depending on the intensity of their strain. This gives the strain on the bond as it shows how much the bond has been forced to change.

$$S_S = \frac{V_{old}(d)}{V_{old}(1)} = \frac{V_{old}(d)}{4E} \qquad (4\text{-}2)$$

To make a composite score, both scores were normalized and added together so that the maximum score was 100 for readability (Eq. 4-3).

$$Score = 50S_S + 5S_T = 50\frac{V_{old}(d)}{V_{old}(1)} + 5\left(10 - \left|T_g - T_a\right|\right) \qquad (4\text{-}3)$$

To maximize material strength and minimize the highlighted issues with bonding, maximizing the score gives a good approximation of the necessary steps, and overall, it gives a good characterization of the bonding quality for a given simulation.

That finishes all numerical methods utilized with this model to simulate the FFF deposition process. All of these elements worked in tandem to produce an accurate recreation of the conditions and processes for the material. Next it is important to briefly treat time iteration and stability regions.

Time Iteration and Stability Regions

The stability of this model proved to be an essential struggle in producing results. The high powers of the Lennard Jones potential are very sharp and can easily send a solution into divergence. Through development of this model, thousands of node sets have exploded (literally) into divergence. Given more time, a complete look at stability regions and implementation of a superior time iteration algorithm (Runge Kutta 4, reverse Euler, etc.) would be immensely beneficial for quality of results and time to compute (another significant roadblock). Currently, due in part to the difficulty of literature on time iteration, stability, and related topics and due more mainly to lack of early consideration for stability as an issue, attempts at implementation have been unsuccessful.

Over the usage of the model, two methods have been explored as potential time iteration algorithms. The first is a simple Euler method, I.E. using a fixed time step. The second is an adaptive time step based on controlling the maximum observed force. It functions by recording the maximum force observed and setting the time step such that the impulse (force multiplied time) is beneath a set level. A similar time step set for velocity was considered but unused. These methods worked to the needs of the project but improving them in the future is a priority. Though a mix was used, curiously the Euler seemed more stable in its applications.

Model Shape

To do any meaningful simulation, the model must construct a matrix of points that are stable given the standard qualitative concepts. The first idea here was the use of a rectilinear grid which turned out to be unstable and prone to slight rotation and collapse, so a hexagonal matrix was implemented as it is much more stable for interactions based on distance. Figure 4 gives an example of the hexagonal grid as implemented into the simulation.

(Fig. 4)
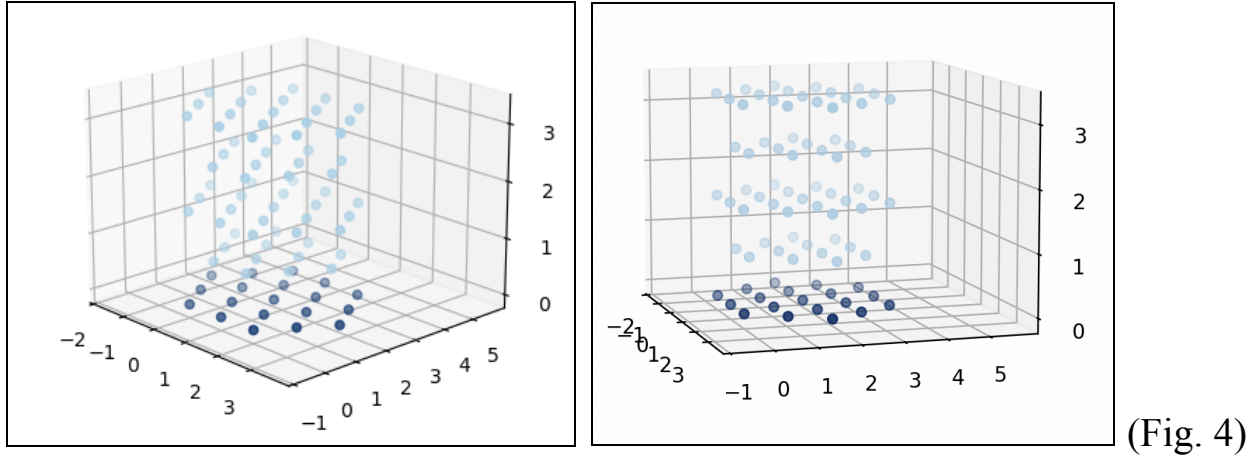
While the setup is fascinating and included some moderately nontrivial geometry, it isn't incredibly pertinent to the actual modeling of the material. The build process is detailed in Appendix A if more information would be beneficial, but the important details are given here. The main principle is that all nodes are equidistant to their neighbors and unlike the rectilinear grid it requires significant force to break. Additionally, a hide feature was included to mask nodes that hadn't been printed yet, so given an extrusion rate, nodes could be gradually introduced into the model, simulating active printing.

Data and Implementation

Finding relevant data and implementing physically realistic material values gave this algorithm the actual realism and applicability needed. The material chosen for specialization and simulation is polylactic acid (PLA), a very common plastic for FFF AM. Although PLA was selected here, the model is flexible for any material for similar use. Here is summarized the data found for PLA and where it was utilized.

First, Thermal Diffusivity of PLA is $5.8244 \cdot 10^{-7} \frac{m^2}{s}$. This is from an industry material information sheet[10] and a formula given in a paper on AM Thermodynamics[11]. This is for implementation in the Heat Exchange calculations.

The Glass Transition Temperature of PLA is 68.5° C. This is from a paper on the general properties of PLA and its uses[12]. A wide spectrum for the values were reported, and they were almost always given as a range of potential values. It seems likely PLA T_g depends on the manufacturer or other sources. This is used for defining phase shifts and property changes.

15

The energy of the attraction (E) is difficult to pin down given the somewhat ambiguous grid. The value is calculated from the tensile strength. Using it, individual maximum force before separation between particles is found using $F = \sigma \cdot A$ as 70 N[13]. Thus, the $F = \frac{dV}{dr}$ is 70 N. Looking at the formula for F, the max force achieved is $2.689901 \cdot E$. Thus, if the desired max force is 70 N, E would be $\frac{70}{2.689901} J = 26.023 J$.

The viscosity of PLA is a bit difficult to find due to its general usage, so the shear modulus, which is easier to find, can be used. Since viscosity is given by shear modulus G times relaxation time λ, viscosity is roughly given by 1.287 MPa[13, 14]. While viscosity does change with temperature. This change was simply considered with the same factor as in the calculation of ε (Eq. 2-2).

The Thermal Expansion of PLA is $4.17 \cdot 10^{-4} K^{-1}$. There is also some flexibility on the specific definition of this constant likely again due to manufacturing differences. This particular value came from a recent paper investigating the thermal expansion of PLA with variable infill[15].

Some additional values used include plate temperature of 50 ºC, extrusion temperature of 110 ºC, and nodal diameter of 1 mm. The first two represent typical and common settings for those two. The last is a computational choice, resulting in a mass per node of 1.24 mg.

These data values bring this model to life with needed realism. Through the effective use of these values, the model is able to simulate FFF and characterize its bonding.

Verification and Validation ------------

The Verification and Validation of this model is crucial to ensure its effectiveness as a means for prediction and generalization. To verify the components of the simulation highlighted in Methodology and Algorithms, individual test simulations show effectiveness of each component in its isolated form. The simulation for thermal energy exchange is a textbook example of heat conduction. As for validation, two general cases, one at high temperature and one at low will illustrate the effective modelling of these different characteristics.

Heat Transfer

Starting off with heat, the popular problem Heat Conduction into an Semi-Infinite Wall will serve as an example. For this simulation all physical interactions are turned off to standardize distance and reduce computational complexity for faster run times. A hexagon of side length 3 particles with a height of 24 levels served as the basis for the simulation. The first level was fixed at a high temperature (called T_s) and the rest of the material was started at a low temperature (called T_0). The temperatures of the other particles were then recorded at periodic intervals to gain an idea of the temperature flow as modelled. Given these parameters, two limitations may be identified. The first being area in the x and y directions. Limited area in these directions deviates from the theoretical ideal by reducing diagonal heat transfer. Closer to the heating surface however, this difference is less noticeable. Thus, more heed will be paid to nodes close to the plate. The second limitation is the limited height of the model, thus eliminating temperature diffusion to infinity. This means that late times when the heat has penetrated the whole solid will be less accurate. Running the model, the following results are returned. Figure 5 shows the average observed temperatures for each of the 24 levels of the solid (with x being the height of the level with the distance between levels being $\sqrt{\frac{2}{3}}$) at times (from the bottom up) 10, 15, 20, 75, 80, 85, 90, and 185 seconds.
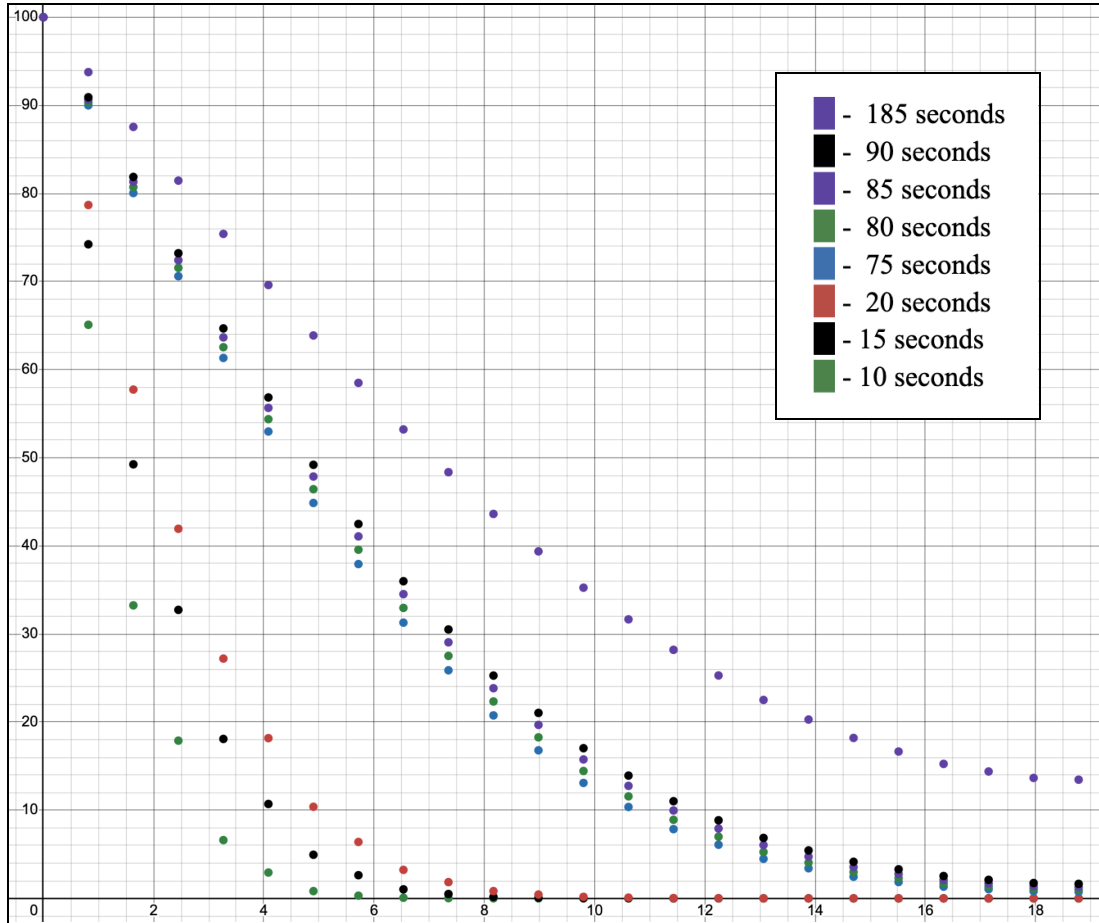
(Fig. 5)

Here can be seen that those limitations did cause the later steps to not exhibit the proper qualitative features. For example, the temperature curve for 185s can be seen to not decay properly to 0 due to the unrealistic stop to the model at 24 levels. This can also be seen (but to a much lesser extent) for the four middle timeframe curves.

To get an idea of how accurate the model is to the theory, a solution curve was mapped to the data points to minimize error given malleable thermal diffusivity, using desmos. Equation 5-1 gives the solution to Heat Conduction into an Semi-Infinite Wall as set out by the physics textbook *Fundamentals of Momentum, Heat, and Mass Transfer*[16]. *x* gives distance in. *t* gives time. α gives thermal diffusivity. *T* is the temperature being solved for. *erf* is the error function.

$$\frac{T-T_0}{T_s-T_0} = 1 - erf\left(\frac{x}{2\sqrt{\alpha t}}\right) \qquad (5\text{-}1)$$

18

Solving for T (Eq. 5-2) gives the function that can be mapped to the results data set.

$$T = \left(T_s - T_0\right)\left(1 - erf\left(\frac{x}{2\sqrt{\alpha t}}\right)\right) + T_0$$ (5-2)

Using desmos to map this function to the data, the following curves are obtained (Fig. 6).

(Fig. 6)
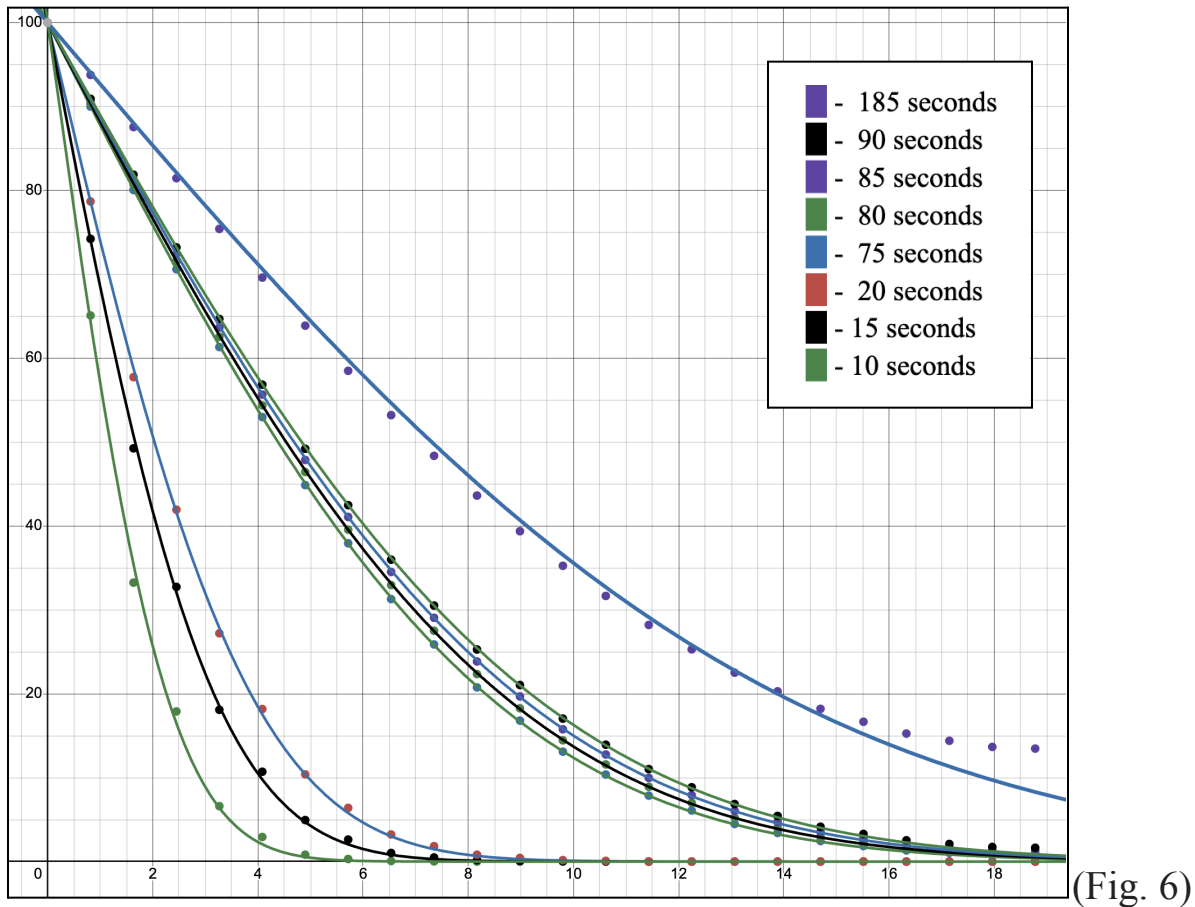
The curves mapped almost all had R² values of 1, though curves near the beginning and end of the timeframe had slightly larger errors. Color unfortunately confuses curves of best fit; the legend is still for the points. Curves in the region described by the limitations exhibited excellent adherence to the actual thermal diffusivity number. The black curve for 15 seconds in the lower three curves is within 1.33% of the actual thermal diffusivity. Curves beyond overestimate the thermal diffusivity, and curves before underestimate it. This is likely due mostly to inaccuracy in

the approximation of the second derivative for the implementation of heat transfer; however, previously described limitations on the scenario also affect the error observed. Overall in the broad and generally-unextreme context of the 3D print environment, the heat transfer mechanism and the 2nd derivative approximation are very accurate and provide a precise input for mechanical changes.

Simple Nodal Interaction

Next, for simple nodal interaction, two particles are placed at 1 mm apart and a separation force is applied to them of 60N, and they should stay together, having their bond stretch accordingly. Running the simulation, the following results are obtained for .5 seconds (Fig. 7). The two particles in the background are for visual distance reference. Saved data was used for accuracy calculations.
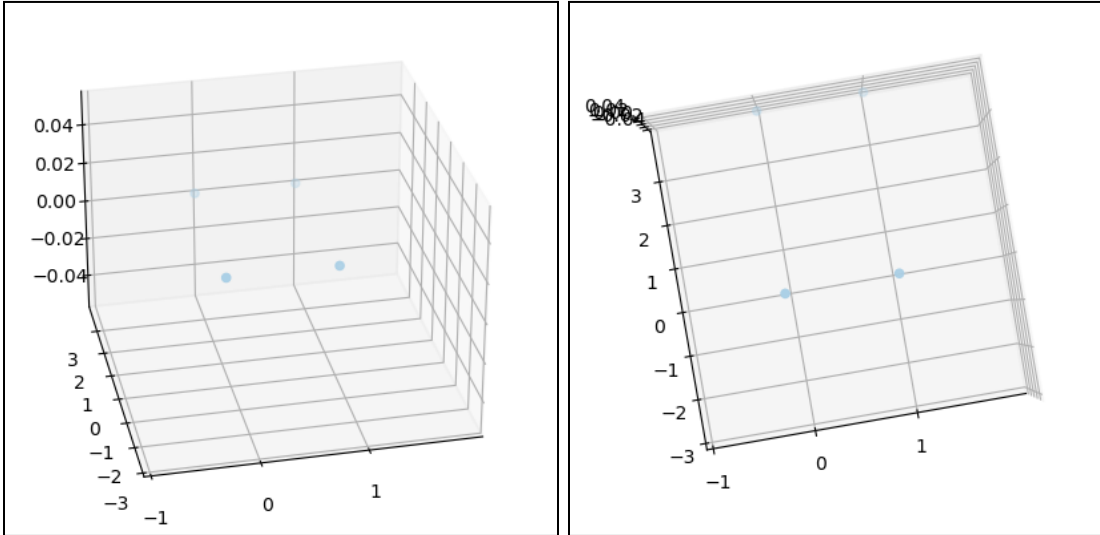
(Fig. 7)

The nodes oscillated in and out due to the initial energy given, but their bond length was easily fit to a sine wave oscillating around 1.04314 mm. That is within 1.3% of the formula ideal. See Figure 8 for the sine wave and plotted points. The x axis is time, and the y axis is bond length.
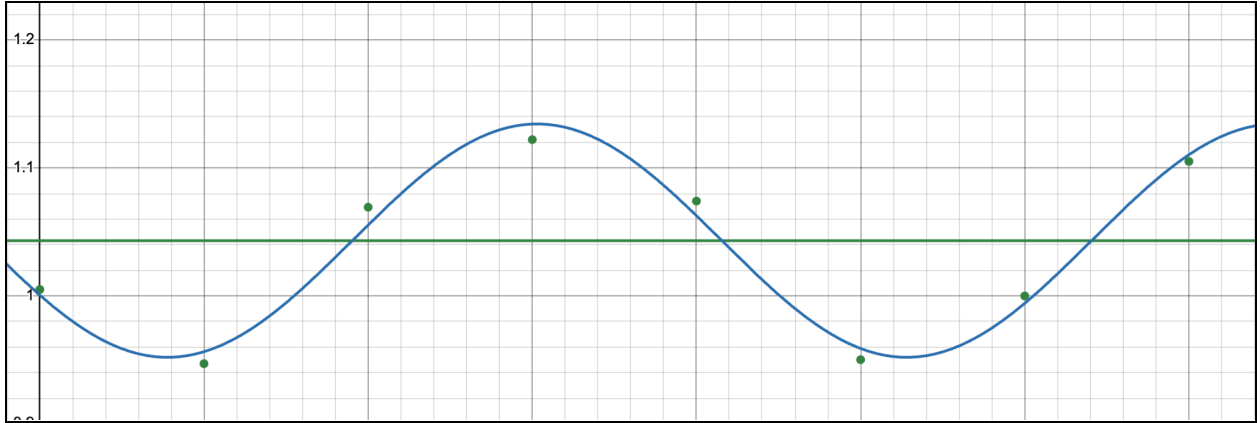
(Fig. 8)

Overall it is evident that the attractive potential is well implemented and calibrated. To illustrate, here is another simulation where the force between these particles is 80N. This simulation was completed over .5 seconds. See Figure 9.
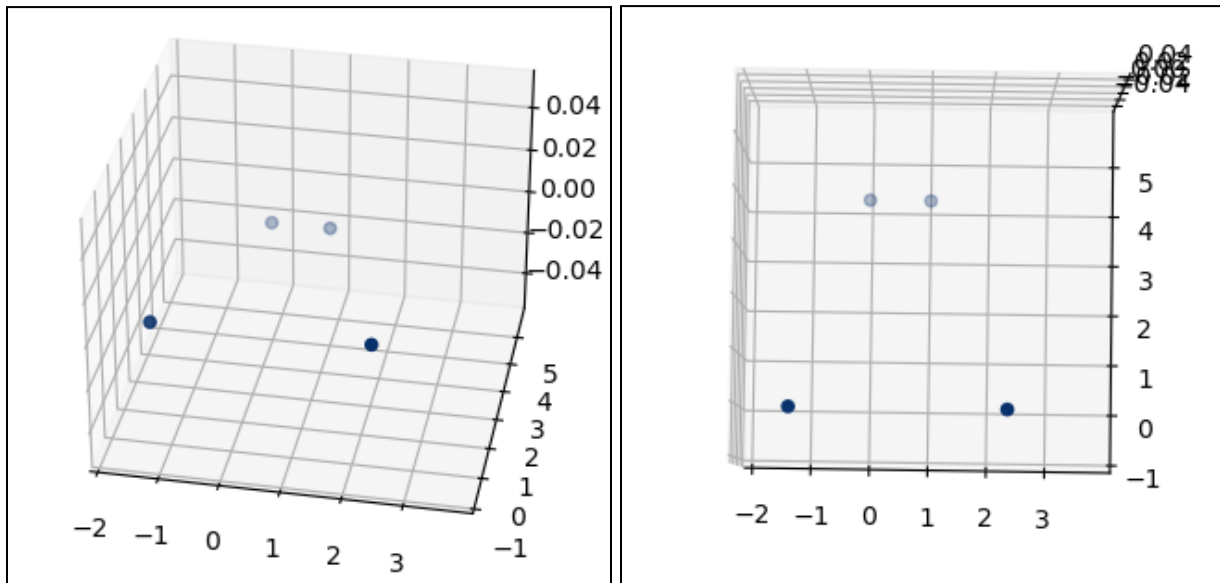
(Fig. 9)

It simulates as intended. The nodes detach and separate.

Complex Nodal Interaction

The next important aspect to test is torque and friction. To do this, three particles are created and placed one millimeter apart in a line on x = 0. The middle particle is fixed positionally (i.e. cannot move but can accumulate angular momentum).Then, one of the outer particles is given a velocity of 1 mm/s. Doing such, the following results are obtained for 1s of simulation (Fig 10).
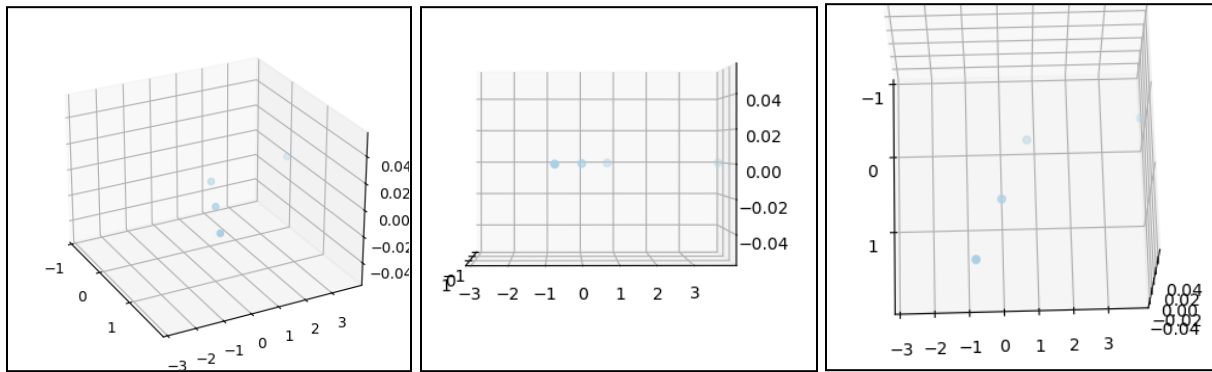
(Fig. 10)

Take note of the backwards motion of the front particle. This is exactly what should happen. This shows the successful effect of the torque and friction within the model and demonstrates the complex interactions under the surface. Despite the simplicity of this simulation, it does a lot to give confidence to the often dense vector algebra calculations that go into its definition.

Repeating the test without fixing the position of the middle particle, a full demonstration of friction can be seen. This simulation also had that initial velocity of 1 mm/s and it was run for 1 seconds. Figure 11 shows the results.

(Fig. 11)

22
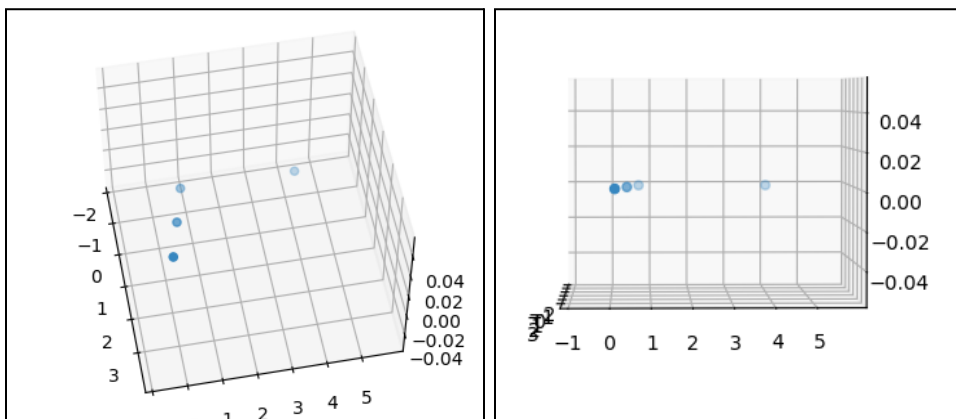
These show how the particles are dragged along as a result of friction. It also shows how the particle doesn't travel the 1mm that it would if it were unimpeded, giving the effectiveness of the friction algorithm.

Now that the effectiveness of the individual components has been explored. Two Validation simulations show how full usage of these algorithms yields correct characteristics. The first of the two simulations is of a low temperature solid. The model shows that it does not move and maintains its shape like a solid. This was run for plastic at 60º C (a bit below the Glass Transition Temperature). Some modifications were needed for this special introduction of solid particles immediately, as calculations for solidification occur after one step of normal consideration (Eq. 2-2 can give extreme values for $T<T_g$). It was run over 2 seconds (small time frame due to computational complexity). Figure 12 gives the results graph on the right and the starting graph (for temperature).
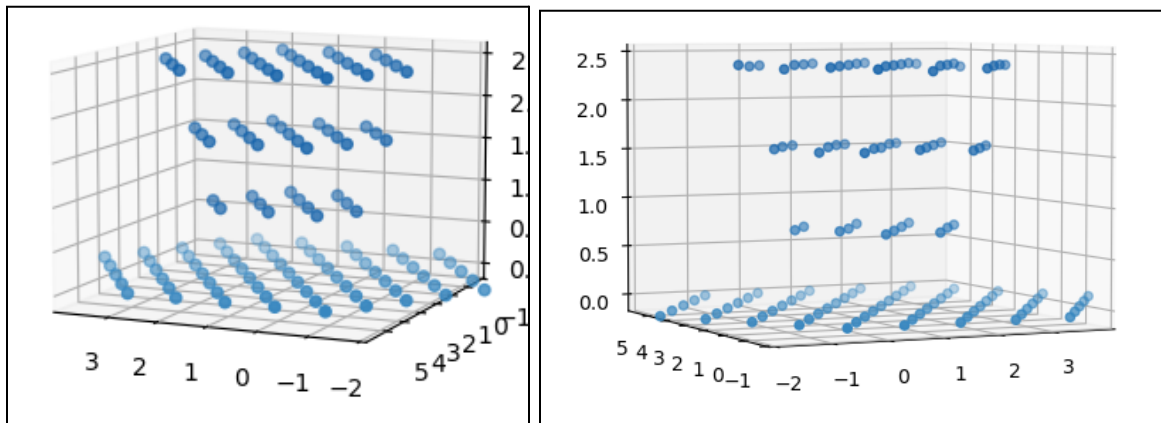
(Fig. 12)

As seen, the model holds its shape successfully. Now, for the second simulation, the material was put at a high temperature and modeled to show liquid characteristics. The temperature was set to 150º C, and it ran over 2 seconds. Figure 13 shows several frames of the results at times 0.75, 1.5, and 2 seconds (left to right). The starting configuration is unshown as it is the same as the previous.

23
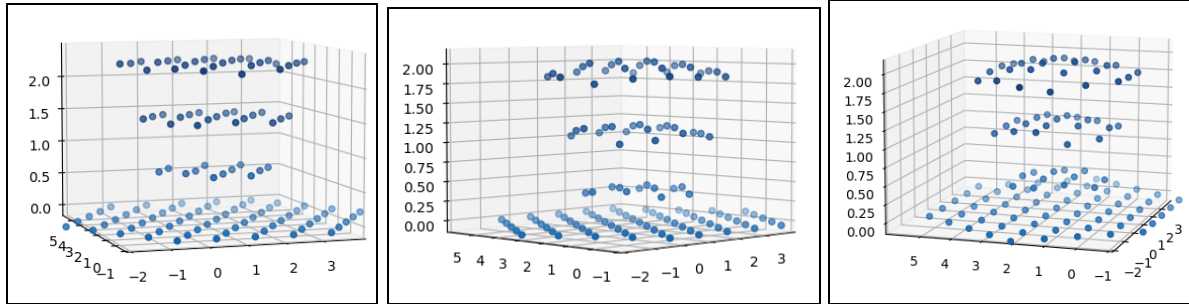
(Fig. 13)

It can be seen clearly that the model successfully models the liquid characteristics of the flow as well. As a qualitative check, a look at the spread of the flow and the actual simulation proportions gives more information about the flow. The actual model is about 6 mm by 6 mm at the start, and it can be seen that the flow spreads from this normally. Given that the surface tension of PLA is low but not infinitesimal at this temperature, it makes sense that the drop (really that's what it is), spreads out a bit but not flowing off the plate yet at 2 seconds in. Longer time wasn't feasible due to long calculation times.

Overall, through these individual verification simulations and these two broader validation simulations, it is clear that the model accurately and effectively models the material in the printing environment.

Results: Analysis and Conclusions -----------

A few experimental simulations were conducted to analyze the effect of various temperature inputs on the quality of bonding and the general conformity to design in the simulation. These simulations showed two major changes to typical practices that would better support model strength and shape.

The first of which is supported by three simulations with varying plate temperatures. Those plate temperatures were 40º C, 60º C, and 65º C. The foremost was to gauge the effects of reducing plate temperature. These simulations yielded significantly better bonding grades for temperatures that are within 10º C of the glass transition temperature. Of course, for plate temperatures too close to the glass transition temperature, slow deformation caused significant structural changes from the design. This, however, was not an issue for temperatures from 5º C

to 10º C lower than the glass transition temperature. Bonding grades were generally 10 to 15 points higher for these high plate temperature simulations. This is supported generally by the concept that actual shifting and movement of the material is very contained and minute. The high viscosity, high tensile strength, and constant solidifying leads the material to be resilient to the small force of gravity on it. This makes focus of proper temperature for bonding significantly more important than keeping overall temperatures low to maintain rigidity. Higher constant temperatures also ensures that the model cools to room temperature uniformly, which, in fact, lowers overall deviance from the design and other physical changes. The usage of higher plate temperatures ultimately supports the effective bonding and the careful adherence to the original shape.

The second major change is more general and related to the laying of material. Due to the often long waits between when filament is applied to an area and when more filament is added to it. Temperature differences can be shocking, leading to poorer bonding and warping and physical changes. To better maintain constant bonding conditions for surfaces to be added to, heating from the top of the model would be beneficial. Sharp temperature changes from very hot added filament to the easily-cooled surroundings nodes causes issues.

In two simulations, changing extrusion temperature gave light to the importance of control for the adding surface. While actually changing the extrusion temperature would be disastrous as the filament would no longer melt and bond properly, this gives light to changing steep temperature changes near that surface. Using lower extrusion temperature, the temperature changes at the adding surface smoothed out and bonding grades went up. To smooth out surface temperatures and provide for better bonding, ventilation at a set temperature would allow finer control. This prevents steep temperature changes, which limit effective bonding and set the stage for unequal thermal contraction. The two simulations were at extrusion temperatures of 95º C and 80º C. By reducing the extremity of the temperature on the bonding side, the bonding grades were observed to go up around 5 to 10 points. It's important to note that this seen change in bonding temperature could reasonably be attributed to a general lowering of the temperature for the model. However, it can be known that this is not the case by considering the previous simulations, showing that raising the overall temperature results in higher bonding grades, so the increase seen is directly from the evening of temperature on the adding side.

These two changes, as seen, benefit the overall strength and adherence to the desired design. Their implementation could improve the effectiveness of FFF processes for myriad applications.

Future Use: Development and Testing -------

The flexibility of this algorithm is key to its importance overall. Using properties from any wide variety of materials, different materials can be modeled without drastic change. This allows this same sort of thermal optimization for any number of applications. Additionally, use on more sophisticated computers with more refined algorithms could yield a significantly more nuanced understanding and, more so, understanding to optimize physical properties.

As for further development of this model specifically, usage of superior time iteration methods, refinement of grid size, and improvement of approximations in second derivatives are priorities for future improvement. Usage of Runge-Kutta or Reverse Euler algorithms for time iteration would significantly improve computation time and likely eliminate bad simulations where a large amount of time is used calculating a simulation only to have it diverge. Refining the grid to smaller particles would make the simulation more accurate, but it would also make the simulation more computationally costly. In the long term, increasing computational cost to increase accuracy is a positive exchange. Lastly, improving approximations in the second derivative by, for example, including more nodes in the approximation or turning the temperature into a field, unbound to nodes, would reduce overall error.

The greatest accomplishment of this process was to model the drag (force from surrounding flow: characterization of friction), torque, and angular momentum of the particles. This utilized difficult implementation of vector algebra and physics, and its inclusion represented an oft unconsidered element of material simulations.

Bibliography and Acknowledgements -------

1 - "Additive Manufacturing Market Size Report, 2030." n.d. Www.grandviewresearch.com.
https://www.grandviewresearch.com/industry-analysis/additive-manufacturing-market.

2 - Pérez, Mercedes, Diego Carou, Eva María Rubio, and Roberto Teti. 2020. "Current Advances
in Additive Manufacturing." *Procedia CIRP* 88 (January): 439–44.
https://doi.org/10.1016/j.procir.2020.05.076.

3 - Fitzgerald, Diana. 2022. "NASA's New Material Built to Withstand Extreme Conditions -
NASA." NASA. April 12, 2022.
https://www.nasa.gov/aeronautics/nasas-new-material-built-to-withstand-extreme-conditi
ons/.

4 - Thomas, Douglas S., and Stanley W. Gilbert. "Costs and Cost Effectiveness of Additive
Manufacturing." *Costs and Cost Effectiveness of Additive Manufacturing*, no. 1176, Dec.
2014, nvlpubs.nist.gov/nistpubs/SpecialPublications/NIST.SP.1176.pdf,
https://doi.org/10.6028/nist.sp.1176.

5 - Javaid, Mohd, et al. "Role of Additive Manufacturing Applications towards Environmental
Sustainability." *Advanced Industrial and Engineering Polymer Research*, vol. 4, no. 4,
Aug. 2021, pp. 312–322,
www.sciencedirect.com/science/article/pii/S254250482100049X,
https://doi.org/10.1016/j.aiepr.2021.07.005.

6 - Gopal, Raghvendra. "What Is a Glass Transition Temperature? - Definition from
Corrosionpedia." *Corrosionpedia*, Corrosionpedia, 2019,
www.corrosionpedia.com/definition/593/glass-transition-temperature-tg.

7 - "A Comprehensive Overview of Injection Molding Cooling Time - Zhongde."
Www.zdcpu.com, 30 June 2023,
www.zdcpu.com/knowledge-hub/injection-molding-cooling-time/.

8 - Li, Yue, et al. "Analysis of Warping Defect Formation Mechanisms in Hot Molding of
CF/PEEK Thin-Wall Structures and Their Influence on Mechanical Properties."
Thin-Walled Structures, vol. 207, 24 Nov. 2024, p. 112740,
www.sciencedirect.com/science/article/abs/pii/S0263823124011807,
https://doi.org/10.1016/j.tws.2024.112740.

9 - S. Fyfitch. *Corrosion and Stress Corrosion Cracking of Ni-Base Alloys*. 1 Jan. 2012, pp. 69–92, https://doi.org/10.1016/b978-0-08-056033-5.00079-3.

10 - *PLA Technical Data Sheet (Polylactic Acid)*. https://www.seas3d.com/MaterialTDS-PLA.pdf

11 - Blanco, Ignazio, et al. "Specific Heat Capacity and Thermal Conductivity Measurements of PLA-Based 3D-Printed Parts with Milled Carbon Fiber Reinforcement." *Entropy*, vol. 24, no. 5, 6 May 2022, p. 654, https://doi.org/10.3390/e24050654.

12 - Khouri, Nadia G, et al. "Polylactic Acid (PLA): Properties, Synthesis, and Biomedical Applications - a Review of the Literature." *Journal of Molecular Structure (Print)*, vol. 1309, 1 Apr. 2024, pp. 138243–138243, https://doi.org/10.1016/j.molstruc.2024.138243.

13 - Shivraj Yeole. "Tensile Testing and Evaluation of 3D Printed PLA Specimens as per ASTM D638 Type-IV Standard." *3rd International Conference on Innovative Design and Development Practices in Aerospace and Automotive Engineering (IDAD 2018)*, 23 Feb. 2018, www.researchgate.net/publication/323726339_Tensile_Testing_and_Evaluation_of_3D_Printed_PLA_Specimens_as_per_ASTM_D638_Type-IV_Standard.

14 - Yi-Sheng Jhao, et al. "A Mechanical Model for Stress Relaxation of Polylactic Acid/Thermoplastic Polyurethane Blends." *Journal of Composites Science*, vol. 8, no. 5, 1 May 2024, pp. 169–169, www.mdpi.com/2504-477X/8/5/169, https://doi.org/10.3390/jcs8050169.

15 - Botean, Adrian - Ioan. "Thermal Expansion Coefficient Determination of Polylactic Acid Using Digital Image Correlation." *E3S Web of Conferences*, vol. 32, 2018, p. 01007, https://doi.org/10.1051/e3sconf/20183201007.

16 - Welty, James R, et al. *Fundamentals of Momentum, Heat, and Mass Transfer*. John Wiley & Sons, 1976.

Benenson, Walter, et al. *Handbook of Physics*. New York, Springer, 2006.

Hesthaven, Jan S, et al. *Spectral Methods for Time-Dependent Problems*. Cambridge University

    Press, 11 Jan. 2007.

John Charles Butcher. *Numerical Methods for Ordinary Differential Equations*. Chichester, West

    Sussex, Wiley, 2016.

Acknowledgements

Appendix A - Building the Hexagonal Grid -

    To build the stable and effective grid for this simulation a hexagonal grid of many equilateral triangles was used. These equilateral triangles had side length one, and the nodes were placed at each vertex. This was pretty simple for the first hexagon. Given some side length n, the first row has n particles of spacing one, the next row has n+1 particles with an offset of ($\frac{-1}{2}, \frac{\sqrt{3}}{2}$) times rows minus one. That offset simply comes from looking at the height and half the base of an equilateral triangle, literally taking the side and turning it into a vector. This holds until there are the same number of rows as there are nodes per side. Then the offset is given as

(1-n+row/2, $\frac{\sqrt{3}}{2}$ row). This comes from carefully considering the definition of this 'line,' as it continues the other. Et voila, the first level is done.

Using some more geometry to make an equilateral triangular prism, the z change between levels is $\sqrt{\frac{3}{2}}$. There is also a new offset which is the vector to the center of the triangle: $(\frac{1}{2}, \frac{1}{2\sqrt{3}})$ or $(0, \frac{1}{\sqrt{3}})$ depending on the orientation of your triangle. The initial choice gives two rotationally equivalent second levels. Alternating between these gives proper progression inward or outward (adding or subtracting them). The node distribution on these layers is a little more complicated since it's not a perfect hexagon, skewing definitions on when to start moving the X offset inward and when to end. These two formulas give the number of nodes per level by hexagonal and in between respectively: $3n^2 - 3n + 1$, $3n^2 - 6n + 3$. n changes from a in between section moving inward. Those formulas can be derived from simple series sum ideas.

The hexagonal matrix overall made the model more stable and more effective at predicting the motion and structure of the solid.